

Influence of Ti target current on microstructure and properties of Ti-doped graphite-like carbon films

WANG Yong-xin^{1,2}, WANG Li-ping¹, XUE Qun-ji¹

1. State Key Laboratory of Solid Lubrication, Lanzhou Institute of Chemical Physics, Chinese Academy of Sciences, Lanzhou 730000, China;
2. Graduate University of Chinese Academy of Sciences, Beijing 100039, China

Received 28 June 2011; accepted 5 September 2011

Abstract: Ti-doped graphite-like carbon (Ti–GLC) films were synthesized successfully by magnetron sputtering technique. The compositions, microstructures and properties of the Ti-doped GLC films dependent on the parameter of Ti target current were systemically investigated by Raman spectra, X-ray photoelectron spectroscopy (XPS), X-ray diffraction (XRD), scanning electron microscopy (SEM), atomic force microscopy (AFM), nanoindentation and ball-on-disk tribometer. With the increase of the Ti target current, the ratio of sp^2 bond and the content of Ti as well as the film hardness and compressive internal stress increase, but the high content of the Ti would result in the loose film due to the formation of the squamose structure. Less incorporated Ti reduces the friction of the GLC film in dry-sliding condition, while pure GLC film exhibits the lowest friction coefficient in water-lubricated condition. Ti–GLC film deposited with low Ti target current shows high wear resistance in both dry-sliding and water-lubricated conditions.

Key words: Ti-doped graphite-like carbon film; microstructure; tribological performance; target current

1 Introduction

Amorphous carbon (a-C) films mainly composed of sp^3 and sp^2 bonds have a great potential to be widely used in modern industry for their attractive properties such as high hardness, high wear resistance and low friction coefficient [1–4]. In order to distinguish the famous a-C films which were named the diamond-like carbon (DLC) according to their relatively high content of sp^3 bonds [5–9], the graphite-like carbon (GLC) film was proposed recently due to its high ratio of sp^2 -hybridized carbon inside the carbonaceous amorphous matrix [10–13]. These studies have demonstrated the high hardness and excellent tribological performance in both the ambient air and water environment for the GLC films. But most of the reported GLC films were the pure carbon matrix without any alloying elements. It was rare to know the influence of the element doping on the microstructure and properties of the GLC films.

On the side, various additive elements have been

alloyed in the amorphous carbon matrixes to improve the mechanical, chemical and tribological properties of DLC films. It was known that the addition of F or Si in DLC films improves the friction and wear due to the beneficial tribochemical reaction on the contact surfaces [14], and the incorporation of H, Ar or N could adjust the microstructure and mechanical properties of DLC films [15], furthermore, the main emphasis had been placed on the doping of Ti, Cr and W in amorphous carbon matrix since they were strong-carbide-forming (SCF) metals and possess an attractive combination of properties (corrosion resistance, wear resistance, etc.) [16–18]. Although above studies had been undertaken to investigate the deposition and properties of DLC films, the research on the Ti-doped GLC composite films, in particular the relationship between the deposition parameters, the mechanical and tribological behaviors has not yet systemically reported.

In this work, Ti-doped graphite-like carbon (Ti–GLC) films were synthesized successfully by magnetron sputtering technique. A middle frequency

power was applied to the twinborn Ti targets for the sputtering of Ti. The evolution of microstructures and properties of Ti–GLC composite films as the function of Ti target current were systematically studied.

2 Experimental

The Ti–GLC composite films were deposited on Si wafer (p-type(100)) and stainless steel by magnetron sputtering deposition process in the argon (Ar) atmosphere. The depositing system was configured three magnetron target positions which focused on a substrate seat. High pure graphite target was fixed in the middle of these target positions, and two twinborn Ti targets were fixed on the other two target positions. A DC power was used on the high-pure graphite target to sputter carbon, while a mid-frequency AC power was applied to the twinborn Ti targets to sputter Ti. Prior to deposition, the substrates were cleaned ultrasonically in ethanol and acetone bathes in succession and dried with a blower. The base pressure of the chamber before deposition was pumped to 1.0×10^{-3} Pa, and the deposition pressure 1.0 Pa was reached with a constant flow of Ar gas. The substrates were DC sputter-cleaned for 15 min at a bias voltage of -1000 V with duty cycle of 50%. Then the interlayers of Ti were pre-deposited to improve the adhesion between the substrates and GLC films. The Ti target current was 2.0 A, while the bias voltage was -500 V with duty cycle of 50%. On the top of the Ti interlayers, GLC films were deposited with incorporation of Ti. Different mid-frequency currents were applied to the Ti targets to adjust the Ti content in the GLC films. The detailed deposition parameters were as follows: an applied DC current of 1.2 A to graphite target, an applied mid-frequency current increased from 0 to 1.0 A to Ti targets, a deposition bias voltage of -300 V (duty cycle 50%), Ar gas flow rate of 50 mL/min, a deposition pressure of 1 Pa and a deposition time of 100 min.

The microstructures of the as-deposited Ti–GLC films were characterized by Raman spectroscopy (Raman, HR800 Raman spectroscopic measurement), X-ray photoelectron spectroscopy (XPS, Perkin-Elmer PHI–5702 multi-functional X-ray photoelectron spectroscope), X-ray diffraction (XRD, Rigaku Dmax 2400 X-ray diffract meter), scanning electron microscopy (SEM, JSM–6701 scanning electron microscope) and atomic force microscopy (AFM, SPM–9500 atomic force microscope). The worn morphology of the contact surfaces of mating balls were investigated by a JSM–5600 SEM.

Nanohardness of each Ti–GLC film was measured by a Nanotest600 nanoindenter apparatus (Micro Materials Ltd., UK). After measuring the bending of the coated Si substrates with a surface profilometer, the

internal stress of the films with different Ti contents was calculated based on the Stoney's equation [19]. The tribological behaviors were tested by a ball-on-disk reciprocating tribo-meter both in dry and water-lubricated conditions. The Si_3N_4 balls were used as a counterpart with a diameter of 3 mm. All the tribological tests were performed under a load of 2 N, while the reciprocating amplitude was 5 mm and the frequency was 5 Hz. After each friction test, the wear volume loss was determined from the wear track profiles which were obtained using a non-contact 3D surface profiler (model MicroMAX™, made by ADE Phase Shift, Tucson, AZ, USA). Then the specific wear rates of all the films were calculated using the equation: $K=V/(SF)$ [20], where V is the wear volume in m^3 , S is the total sliding distance in m and F is the normal load in N. The resulted specific wear rate of each film was obtained by averaging four wear tests under the same condition.

3 Results and discussion

3.1 Microstructure of Ti–GLC films

Raman spectroscopy is a standard tool for the characterization of carbon materials [21]. Typical Raman spectrum of a-C usually shows a D peak and a G peak, which lie at around 1350 and 1560 cm^{-1} , respectively [22–24]. The G peak is due to the bond stretching of all pairs of sp^2 atoms in both rings and chains, while the D peak is due to the breathing modes of sp^2 atoms in rings [24]. Because of the different ratios of sp^2 bonds or sp^3 bonds in various a-C films, the location and intensity of the two peaks are different. The enhancement of D peak and the increase of spectrum intensity ratio I_D/I_G can be considered the evidence of the increase in graphite structure (sp^2 bond), which was also named as graphitization for the a-C films [25,26]. The Raman spectra of the as-deposited Ti–GLC films are shown in Fig. 1. As shown in Fig. 1, the intensity of D peak increases drastically with increasing the mid-frequency current on Ti targets, and the value of I_D/I_G shown in Fig. 2 greatly increases from 1.7 to 4.0 as the Ti target current increases from 0 to 0.8 A, and then the value of I_D/I_G suddenly increases to 10.0 as the Ti target current increases to 1.0 A, which indicates that the ratio of sp^2 bonds increases in the meantime. The weakened Raman signals of the films with high Ti target current might be related to the decrease of the carbon inside the as-deposited films. The weakened Raman signals of the films with high Ti target current might be related to the decrease of the carbon inside the as-deposited films.

The C1s spectra of Ti–GLC films with different Ti target currents acquired from the XPS analysis are shown in Fig. 3. It can be clearly seen that the bond shifts

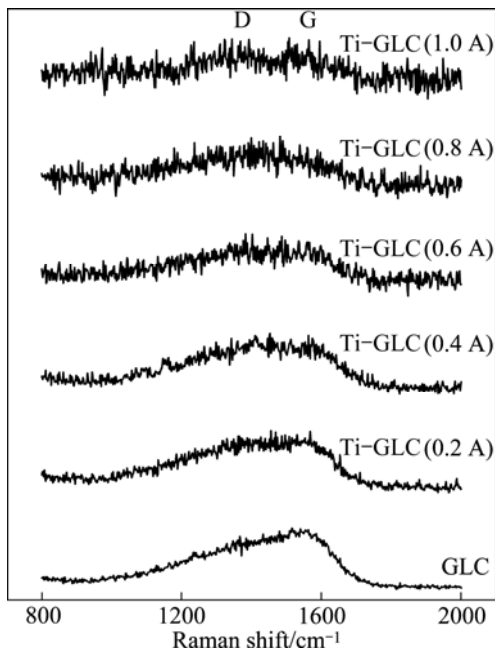


Fig. 1 Raman spectra of Ti-GLC films at different Ti target currents

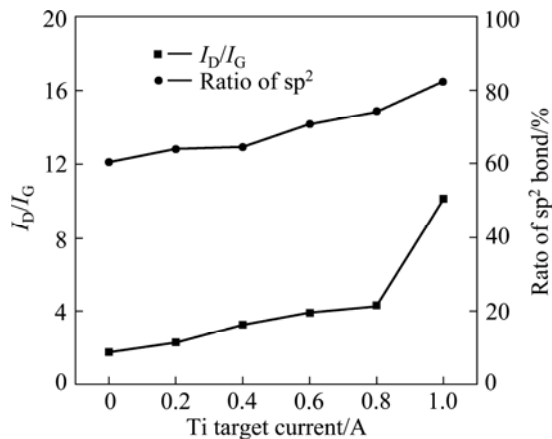


Fig. 2 I_D/I_G and ratio of sp^2 bonds in carbon of Ti-GLC films

towards lower binding energy with the increase of Ti target current, which indicates that the ratio of sp^2 bond in carbon increases due to the relatively low binding energy of sp^2 (284.4 eV) compared with sp^3 bond (285.2 eV) [27,28]. In detail, since the intensity of the binding energy is linearly proportional to the fraction of sp^2 and sp^3 bonds, the ratio of the sp^2 bond of the carbon inside the as-deposited Ti-GLC films can be calculated approximately after peak fitting shown in Fig. 2. The result shows that the ratio of sp^2 bonds increases from 61% to 82% with the Ti target current increasing from 0 to 1.0 A. This result supports the Raman analysis, indicating the graphitization effect of GLC films during the Ti target current increasing, which can be attributed to the following two factors. One is the increase of

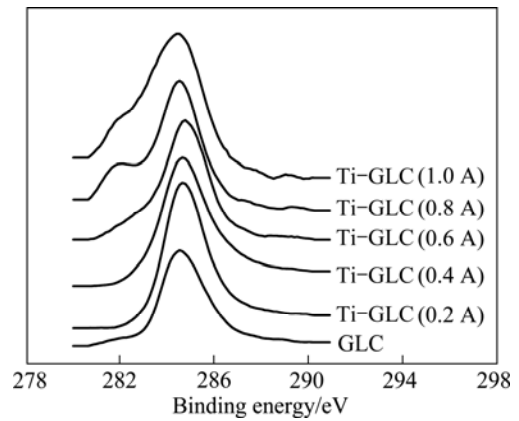


Fig. 3 C1s spectra of Ti-GLC films at different currents

temperature resulting from the enhanced ions bombarding; the other is the incorporation of Ti in carbon matrix [29]. Figure 4 demonstrates that the temperature inside the vacuum chamber and the content of Ti in Ti-GLC film both increase with the increase of Ti target current. As shown in Fig. 4, the temperature in the vacuum chamber increases from approximately 58 to 105 °C as the Ti target current increases from 0 to 1.0 A. Since the heat transmission in vacuum is very limited, the temperature on the surface should be relatively high. The enhanced temperature during the deposition process leads to the transformation from sp^3 bond to sp^2 bond since the sp^3 carbon phase is thermodynamically less stable than the sp^2 carbon phase [30], promoting the increase of sp^2 bonds in carbon matrix. In another view point, higher target current supplies more Ti ions incorporated in a-C films which can cause damage by breaking some of the sp^3 bonds, leading to the formation of a stable sp^2 -bonded phase. The contents of Ti in the as-deposited Ti-GLC films calculated from the XPS analysis are also shown in Fig. 4. As seen from Fig. 4, the content of Ti increases from 0 to 20% as the Ti target current increases from 0 to 1.0 A, thereby to increase the ratio of sp^2 bonds in the carbon matrix [31].

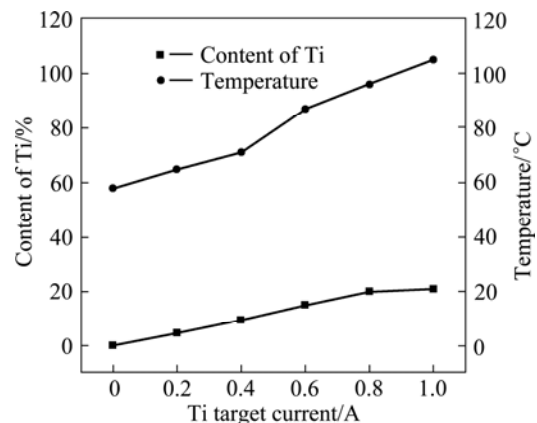


Fig. 4 Content of Ti in Ti-films and temperature in vacuum chamber

The increase of Ti can be separated into two stages due to the different chemical states revealed from XPS spectra in Fig. 3 and XRD analysis in Fig. 5. At the first stage, Ti was incorporated in the carbon matrix as a simple substance when the Ti target current was low. At the second stage, the compound of TiC was formed when Ti target current increased to be high. Seen from Fig. 3, the C1s spectra do not exhibit the peak feature of TiC binding energy posited at 281.7 eV for films deposited with Ti target current of 0, 0.2 and 0.4 A, which is considered that no TiC is synthesized under these conditions. It was further sustained by the XRD analysis shown in Fig. 5. Besides pure GLC film deposited without Ti target current cannot have Ti, the XRD spectra of Ti–GLC films deposited with Ti target current of 0.2 and 0.4 A shown in Fig. 5 only exhibit weak peaks consisted of Ti (101) or/and (110), suggesting that Ti exists as a simple substance in the corresponding films. Whereas, the peak features of TiC in XPS spectra are able to be seen clearly in Fig. 3 when the Ti target current increases to 0.6 A, as well as the XRD diffraction peaks TiC (111), (200), (220) or (311) are revealed in Fig. 5, indicating that the compound of TiC is successfully synthesized in this condition. The evolution of chemical state for Ti must be related to the increase of Ti target current, which means the increase of the Ti target current. When the Ti target power is lower, ions of Ti sputtered from Ti targets cannot bond with ions of C sputtered from graphite target due to their low energy and quantity. Only if the energy and quantity of Ti ions

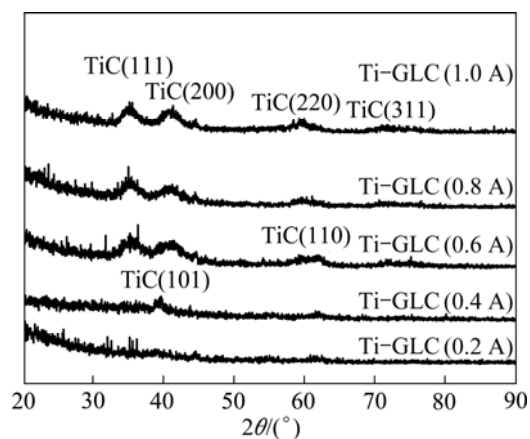


Fig. 5 XRD patterns of Ti–GLC films

increased to the threshold with increasing Ti target power, the Ti bond with C can form compound of TiC.

The content as well as the chemical state variations of Ti as a function of Ti target current also resulted in the evolution of the surface morphologies of the as-deposited Ti–GLC films. When Ti target current was low, a little of Ti incorporating in the amorphous carbon matrix could not destroyed the freely bonding between C atoms markedly, resulting in dense films in this condition. However, not only did the content of Ti increase gradually with increasing Ti target current but also the compound of TiC was formed, promoting the preferred orientation growing in the as-deposited Ti–GLC films with high Ti target current. As seen in Fig. 6, the surface of Ti–GLC deposited with high Ti target current is looser

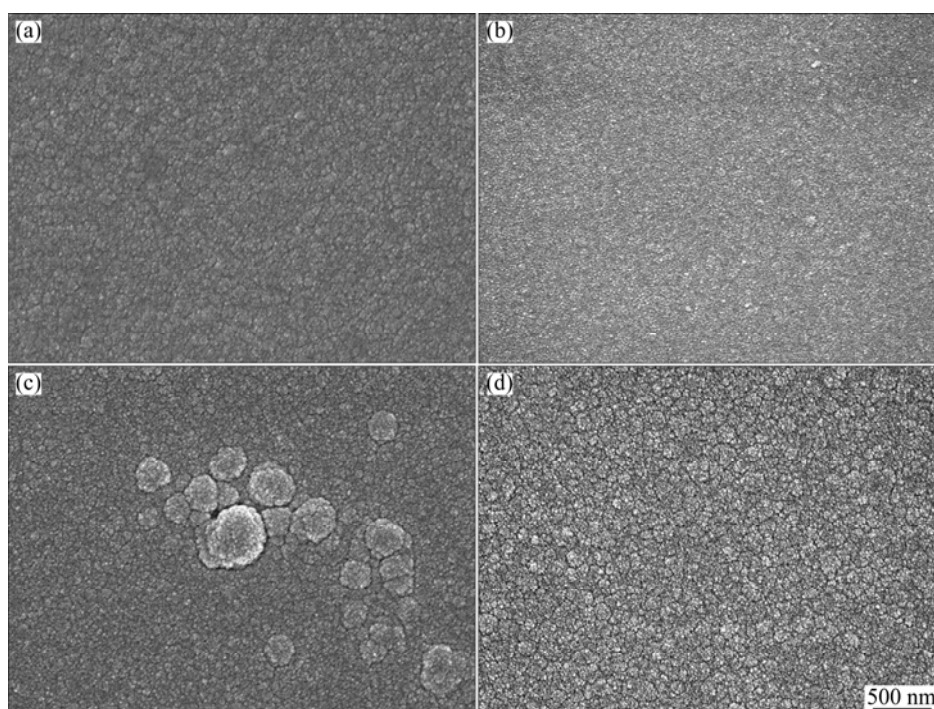


Fig. 6 Typical SEM images of Ti–GLC films at different Ti target currents: (a) 0 A; (b) 0.6 A; (c) 0.8 A; (d) 1.0 A

than that deposited with low Ti target current. Moreover, some loose areas with large particles on the surface of film deposited with Ti target current 0.8 A can be seen in Fig. 6(c), while film deposited with Ti target current of 1.0 A exhibits a typical squamose structure shown in Fig. 6(d).

The evolution of surface roughness investigated by AFM is shown in Fig. 7, and some of the surface morphologies are given in Fig. 8. It is clearly seen from Fig. 7 that the roughness decreases from 2.5 to 1.4 nm when Ti target current increases from 0 to 0.2 A, and the 3D AFM morphology of Ti–GLC film deposited with Ti target current of 0.2 A reveals smaller particles than pure GLC film deposited without Ti (as shown in Figs. 8(a) and (b)). Whereas, the roughness of the as-deposited Ti–GLC films increases gradually after the Ti target current increases to 0.2 A, while the increase of the particle size on 3D AFM morphologies in the same order is observed (Figs. 8(c) and (d)). It can be considered that a little of Ti doped with low Ti target current smooths the surface of GLC film, but the surface roughness increases drastically with increasing Ti target current in the high range.

3.2 Mechanical and tribological performance of Ti–GLC films

Nanohardness and internal stresses of Ti–GLC films deposited at different Ti target currents are shown in

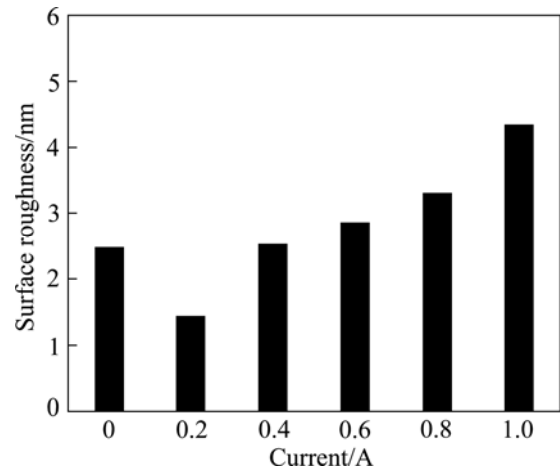


Fig. 7 Roughness of Ti–GLC films

Fig. 9. As seen in Fig. 9, the nanohardness increases from 16 to 22 GPa as Ti target current increases from 0 to 0.4 A, and then, fluctuates slightly around 22 GPa till Ti target current increases to 0.8 A. The highest nanohardness of 24 GPa was obtained when film was deposited at 1.0 A. The evolution of film hardness must be highly related to the content of Ti and its bonding state with C, which resulted in the variation of internal stress, as shown in Fig. 9. Seen from Fig. 9, the negative value suggests a kind of compressive internal stress, which increases from 0.5 to 1.2 GPa as the Ti target

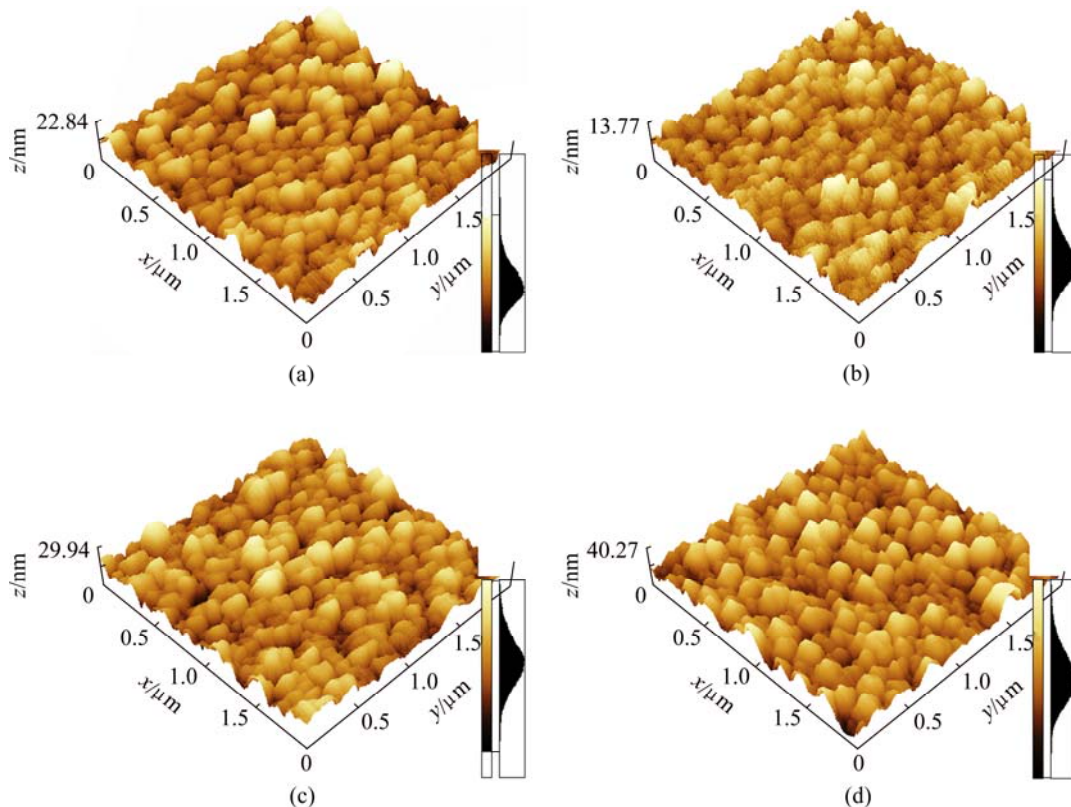


Fig. 8 AFM morphologies of Ti–GLC films at different Ti target currents: (a) 0 A; (b) 0.6 A; (c) 0.8 A; (d) 1.0 A

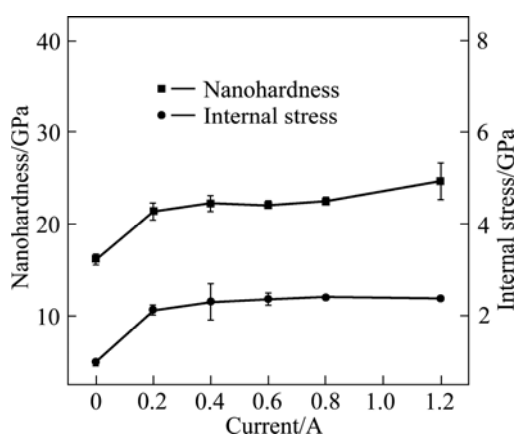


Fig. 9 Nanohardnesses and internal stress of Ti-GLC films

current increases from 0 to 0.4 A due to the exotic element of Ti embedded in the carbon matrix increases from 0 to 10 %. The enhanced compressive internal stress increased cohesion of the as-deposited GLC film, resulting in the high resistance under pressure. Thus the hardness of the film was increased with the increase of the compressive internal stress. However, though the content of Ti increases gradually, the compressive internal stress does not increase after Ti target current increases to 0.6 A, as seen in Fig. 9, which can be attributed to the well linking between the Ti atoms and the carbon matrix due to the formation of TiC. The changeless compressive internal stress made the nanohardness vary slightly after the Ti target current increases to 0.6 A. The highest hardness of 24 GPa for film deposited with Ti target current of 1.0 A might be related to its high content of hard TiC particles.

The friction coefficients of Ti-GLC films with different Ti target currents in both dry and water-lubricated conditions are shown in Fig. 10. In dry-sliding condition, it can be seen clearly that the friction coefficient of pure GLC film deposited without Ti is 0.063, and the friction coefficient of GLC doped 5% Ti using Ti target current of 0.2 A is reduced to 0.043. However, the friction coefficient of the as-deposited Ti-GLC films increases to 0.105 gradually as the Ti target current increases to 1.0 A. This variation of friction coefficient might be related to the evolution of surface roughness as well as the microstructure of the as-deposited films. Compared Fig. 10 with Fig. 7, the variations of roughness and friction coefficient of the Ti-GLC films in ambient air are similar. Obviously, low roughness gives the low friction coefficient due to the low friction shear resistance of the smooth film surface. However, the surface roughness of wear tracks will be changed certainly after running-in period. Here, the evolution of microstructure must be the deep reason to the developing of friction coefficient in ambient air. With

the increase of Ti target current, the graphitization effect for Ti-GLC films resulted in the increase of the sp^2 bond in carbon, whereas, the content of C of Ti decreased or increased. The increase of the sp^2 bond enhanced the solid lubricating effect of the GLC films due to the weak adhesion of π bond in sp^2 -hybridized carbon on the film surface, but the increase of Ti content in the high range will increase the friction shear resistance. The two opposite effects make the lowest friction coefficient of Ti-GLC films perform when the Ti is incorporated at a low target current of 0.2 A.

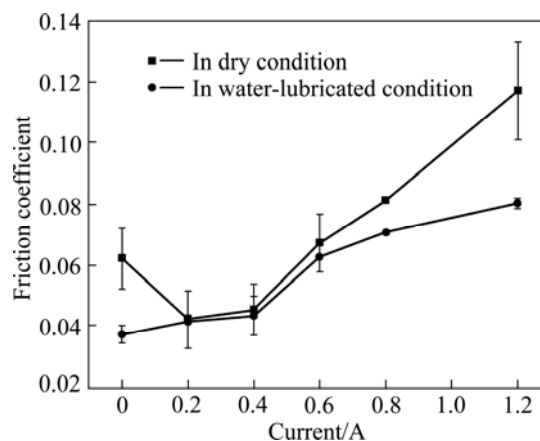


Fig. 10 Friction coefficients of Ti-GLC films at different Ti target currents

However, the friction coefficient of Ti-GLC film in water-lubricated wear condition increases from 0.036 to 0.075 gradually as the Ti target current increases from 0 to 1.0 A, as seen from Fig. 10. Additionally, each of the friction coefficients in water-lubricated wear condition is lower than that in dry-sliding condition for the same film. All can be attributed to the mutual effect between the solid lubricating and hydraulic lubricating. According to the present studies [32,33], one of the most effective solid lubricating effects of amorphous carbon was the formation of transferred tribolayer on mating surface. From Fig. 11(a), the thick lubricating transferred tribolayer on the contact surface of mating Si_3N_4 ball can be seen clearly when sliding in dry condition. But only a few of transferred materials can be seen on the edge of the wear scar of the mating Si_3N_4 ball in water-lubricated wear condition (Fig. 11(b)), which suggests that water prevents the formation of the transferred tribolayer, resulting in the little significance of bonding structure in carbon to the friction shear resistance in water-lubricated wear condition. In addition, the surface roughness cannot affect the friction coefficient of amorphous films in the short running in period in water. Therefore, the variation of friction coefficient in water-lubricated condition is only affected by the content of C or Ti, which makes the friction coefficient increase gradually with the decrease

or increase of C/Ti. However, it is certainly that the water hydraulic lubricating effect reduces the friction shear resistance effectively, resulting in the lower friction coefficient in water-lubricated condition than in dry-sliding condition.

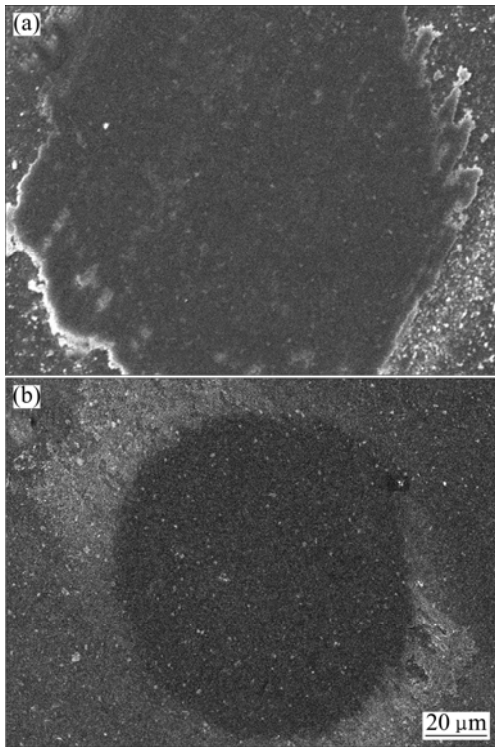


Fig. 11 Contact surfaces of Si_3N_4 balls mated with pure GLC film: (a) In dry-sliding condition; (b) In water-lubricated condition

The corresponding specific wear rates for films deposited with different Ti target currents are shown in Fig. 12. It can be seen that the wear rate of Ti-GLC film fluctuates slightly in the low range till the Ti target current increases to 0.4 A, while it will increase drastically when Ti target current increases to 0.6 A in both the ambient air and water environments. Meanwhile, the wear rate in water-lubricated wear condition is much lower than that in dry-sliding condition as the Ti target current varies from 0 to 0.4 A for the same film, but it will be much higher than that in dry-sliding condition when the Ti target current increases to 0.6 A. The lowest wear rate in dry-sliding condition is approximately $4.5 \times 10^{-16} \text{ m}^3/(\text{N}\cdot\text{m})$, and the lowest wear rate in water-lubricated condition is around $2.0 \times 10^{-16} \text{ m}^3/(\text{N}\cdot\text{m})$. All of that were obtained from the Ti-GLC films deposited with Ti target current less than 0.4 A.

Besides different friction shearing, the variation of wear rates must be highly related to the film density and the different wear mechanisms in dry and water-lubricated conditions. According to the discussion above, the Ti-GLC films deposited with high Ti target current were looser than those deposited with low Ti

target current. Some loose regions or the squamose structure of Ti-GLC films deposited with high Ti target current would be destroyed easily, especially when the friction shear was enhanced in the same time, resulting in severe wear in dry-sliding condition. Seen from Fig. 13, the wear track of film deposited with Ti target current of 0.6 A in dry-sliding condition (Fig. 13(b)) is wider and deeper than film deposited with Ti target current 0.4 A in dry-sliding condition (Fig. 13(a)). Additionally, grooves in wear tracks under dry-sliding condition reveal a plough action during wear, thus the wear mechanism of Ti-GLC films in dry-sliding condition might be assigned to the abrasive wear.

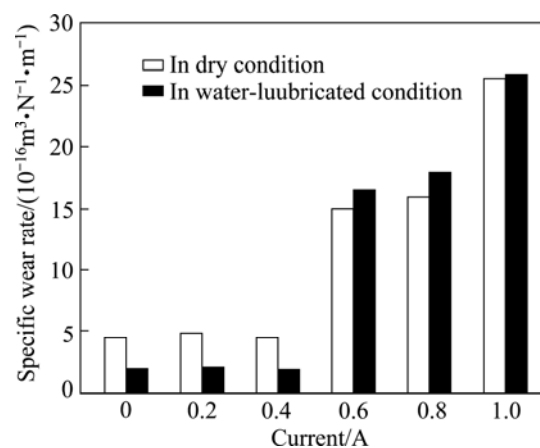


Fig. 12 Specific wear rates of Ti-GLC films

In water-lubricated wear condition, the density of films affected the wear more profoundly. Since the film was dense when deposited with low Ti target current, the water hydraulic lubricating effect resulted in the low friction shear and adhesivity between the contact surfaces, which decreased the wear rates of the as-deposited films. Seen from Fig. 13, the wear track of film deposited with low Ti target current of 0.4 A in water-lubricated wear condition (Fig. 13 (c)) is narrower and shallower than that in dry-sliding wear condition (Fig. 13 (a)). But if the film was loose, the water molecules were apt to infiltrate into the film. Combined with the alternating stress, the erosion of water molecules promoted the initiation and growth of the microcracks more easily in the loose films, leading to the severe wear of the Ti-GLC films. Additionally, if the water molecules went along with the interfaces between particles till to the interface between the interlayer and substrate, the penetrating microcracks were formed, consequently, the brittle failure in some areas occurred. Seen from Fig. 13, the wear track of film deposited at high Ti target current of 0.6 A in water-lubricated wear condition (Fig. 13 (d)) is wider and deeper than that in dry-sliding condition (Fig. 13 (c)), furthermore, the deep holes were observed on the corresponding wear surface.

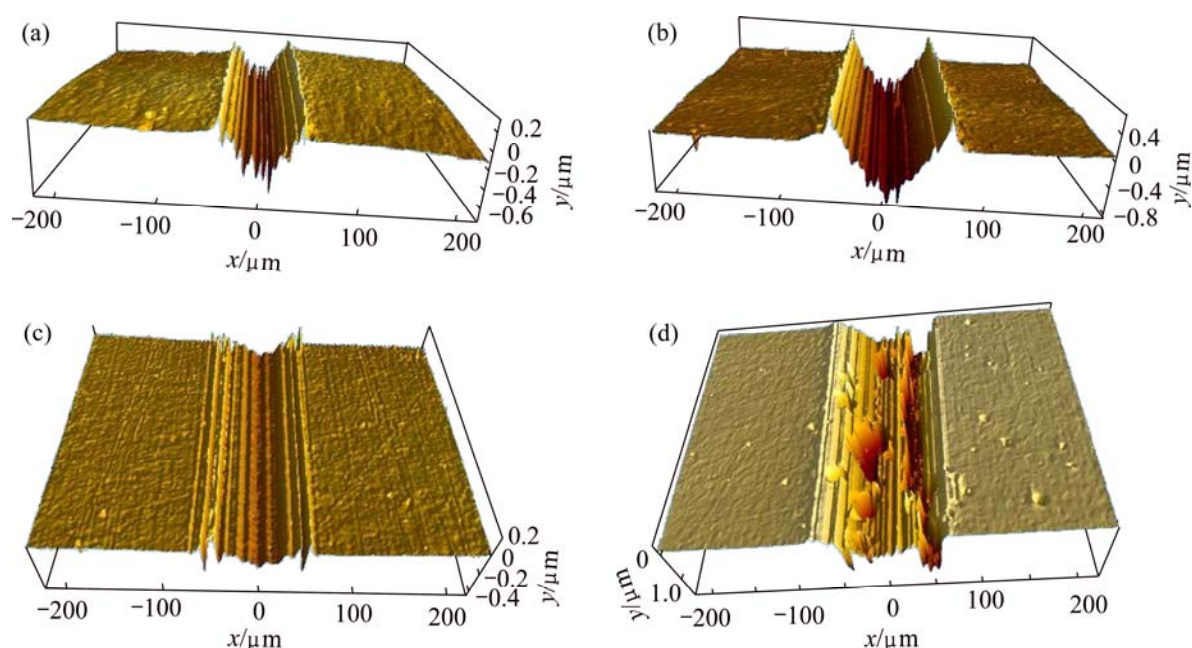


Fig. 13 3D morphologies of wear tracks: (a) Film deposited at 0.4 A in dry-sliding condition; (b) Film deposited at 0.6 A in dry-sliding condition; (c) Film deposited at 0.4 A in water-lubricated wear condition; (d) Film deposited at 0.6 A in water-lubricated wear condition

However, the groove feature in wear tracks for Ti–GLC films both deposited at low or high Ti target currents can be observed in water-lubricated condition, illustrating that the plough action also exists in this condition. Therefore, the wear mechanism in water-lubricated condition is predominated by plough and fatigue wear simultaneously.

4 Conclusions

1) With the increase of the Ti target current, the ratio of graphite structure (sp^2 bonds) in carbon and the content of Ti increase, but the films become loose. Less Ti doped can smooth the GLC film.

2) The hardness increases drastically when Ti target current increases in the low range and is affected slightly when the Ti target current varies in the high range, which is highly related to the content of Ti and its bonding state.

3) Less incorporated Ti under low target current reduces the friction of the GLC film in dry-sliding condition, while pure GLC film without Ti exhibits the lowest friction coefficient in water-lubricated condition. Ti–GLC film deposited with low Ti target current shows high wear resistance in both dry-sliding and water-lubricated conditions. The abrasive wear is in control in the dry-sliding condition, while the wear of Ti–GLC films in water-lubricated condition is attributed to plough action accompanied with the fatigue wear mechanism.

Acknowledgements

The authors acknowledge LIN Zhi of University of Science and Technology Beijing for the measurement of the nanoindentation discussed in this work.

References

- [1] HOLMBERG K, RONKAINEN H, LAUKKANEN A, WALLIN K. Friction and wear of coated surfaces—scales, modelling and simulation of tribomechanisms [J]. *Surf Coat Technol*, 2007, 202: 1034–1049.
- [2] NEVILLE A, MORINA A, HAQUE T, VOONG M. Compatibility between tribological surfaces and lubricant additives—How friction and wear reduction can be controlled by surface/lube synergies [J]. *Tribol Int*, 2007, 40: 1680–1695.
- [3] XIAO Jian-rong, LI Xin-hai, WANG Zhi-xing. Effects of nitrogen content on structure and electrical properties of nitrogen-doped fluorinated diamond-like carbon films [J]. *Transactions of Nonferrous Metals Society of China*, 2009, 19(6): 1551–1555.
- [4] PARK Y, HONG B. Characteristics of sputtered amorphous carbon films prepared by a close-field unbalanced magnetron sputtering method [J]. *J Non-Cryst Solids*, 2008, 354: 5504–5508.
- [5] NOBILI L, MAGAGNIN L. DLC coatings for hydraulic applications [J]. *Transactions of Nonferrous Metals Society of China*, 2009, 19(4): 810–813.
- [6] VANHULSEL A, VELASCO F, JACOBS R, L EERSELS, HAVERMANS D, ROBERTS E W, SHERRINGTON I, ANDERSON M J, GAILLARD L. DLC solid lubricant coatings on ball bearing for space applications [J]. *Tribol Int*, 2007, 40: 1186–1194.
- [7] KULIKOVSKY V, BOHÁČ P, VORLIČEK V, DEINEKA A, D CHVOSTOVÁ, KURDYUMOV A, JASTRABÍK L. Oxidation of graphite-like carbon films with different microhardness and density [J]. *Surf Coat Technol*, 2003, 174–175: 290–295.
- [8] LI Hong-xuan, XU Tao, WANG Cheng-bing, CHEN Jian-min,

- ZHOU Hui-di, LIU Hui-wen. Tribochemical effects on the friction and wear behaviors of a-C:H and a-C films in different environment [J]. Tribol Int, 2007, 40: 132–138.
- [9] RONKAINEN H, VARJUS S, HOLMBERG K. Tribological performance of different DLC coatings in water-lubricated conditions [J]. Wear, 2001, 249: 267–271.
- [10] LACERDA R G, HAMMER P, LEPIENSKI C M, ALVAREZ R, MARQUES F C. Hard graphitic-like amorphous carbon films with high stress and local microscopic density [J]. J Vac Sci Technol A, 2001, 19: 971–975.
- [11] FIELD S K, JARRATT M, TEER D G. Tribological properties of graphite-like and diamond-like carbon coatings [J]. Tribol Int, 2004, 37: 949–956.
- [12] KULIKOVSKY V, METLOV K, KURDYUMOV A, BOHAC P, JASTRABIK L. Study of the structure of hard graphite-like amorphous carbon films by electron diffraction [J]. Diamond Relat Mater, 2002, 11: 1467–1471.
- [13] VIANA G A, LACERDA R G, FREIRE F L Jr, MARQUES F C. ESR investigation of graphite-like amorphous carbon films revealing itinerant states as the ones responsible for the signal [J]. J Non-Cryst Solids, 2008, 354: 2135–2137.
- [14] WU X, OHANA T, TANAKA A, KUBO T, H NANA O, MINAMI I, MORI S. Tribochemical reaction of Si-DLC coating in water studied by stable isotopic tracer [J]. Diamond Relat Mater, 2008, 17: 147–153.
- [15] ZHANG Rui-jun, MA Hong-tao. Nano-mechanical properties and nano-tribological behaviors of nitrogen-doped diamond-like carbon (DLC) coatings [J]. J Mater Sci, 2006, 41: 1705–1709.
- [16] SU Y L, KAO W H. Tribological behavior and wear mechanisms of Ti-C:H/TiC/TiCN/TiN/Ti coatings when sliding against steel, bronze and aluminum alloy rods [J]. J Mater Sci, 2001, 36: 189–199.
- [17] SINGH V, JIANG J C, MELETIS E I. Cr-diamond like carbon nanocomposite films: Synthesis, characterization and properties [J]. Thin Solid Films, 2005, 489: 150–158.
- [18] WANG Xue-min, WU Wei-dong, LI Sheng-yin, BAI Li, CAO Lin-hong, CHEN Song-lin, TANG Yong-jian. Properties of W incorporated diamond-like carbon films prepared by pulsed-laser deposition [J]. J Alloys Compd, 2009, 479: 741–745.
- [19] BAN M, HASEGAWA T. Internal stress reduction by incorporation of silicon in diamond-like carbon films [J]. Surf Coat Technol, 2002, 162: 1–5.
- [20] WANG Li-ping, ZHANG Jun-yan, ZENG Zhi-xiang, LIN Yi-ming, HU Li-tian, XUE Qun-ji. Fabrication of a nanocrystalline Ni-Co/CoO functionally graded layer with excellent electrochemical corrosion and tribological performance [J]. Nanotechnology, 2006, 17: 4614–4623.
- [21] PISCANEC S, MAURI F, FERRARI A C, LAZZERI M, ROBERTSON J. Ab initio resonant Raman spectra of diamond-like carbons [J]. Diamond Relat Mater, 2005, 14: 1078–1083.
- [22] GILKES K W R, PRAWER S, NUGENT K W, ROBERTSON J, SANDS H S, LIFSHITZ Y, SHI X. Direct quantitative detection of the sp³ bonding in diamond-like carbon films using ultraviolet and visible Raman spectroscopy [J]. J Appl Phys, 2000, 87: 7283–7289.
- [23] FERRARI A C, ROBERTSON J. Resonant Raman spectroscopy of disordered, amorphous, and diamondlike carbon [J]. Phys Rev B, 2001, 64: 075414–075426.
- [24] CASIRAGHI C, FERRARI A C, ROBERTSON J. Raman spectroscopy of hydrogenated amorphous carbons [J]. Phys Rev B, 2005, 72: 085401–085414.
- [25] ROBERTSON J. Diamond-like amorphous carbon [J]. Mater Sci Eng R, 2002, 37: 129–281.
- [26] CHIU S M, LEE S C, WANG C H, TAI F C, CHU C W, GAN D. Electrical and mechanical properties of DLC coatings modified by plasma immersion ion implantation [J]. J Alloys Compd, 2008, 449: 379–383.
- [27] LIAO J X, LIU W M, XU T, XUE Q J. Characteristics of carbon films prepared by plasma-based ion implantation [J]. Carbon, 2004, 42: 387–393.
- [28] RYBACHUK M, BELL J M. Electronic states of trans-polyacetylene, poly(p-phenylene vinylene) and sp-hybridised carbon species in amorphous hydrogenated carbon probed by resonant Raman scattering [J]. Carbon, 2009, 47: 2481–2490.
- [29] ZHANG S, BUI X L, FU Y. Magnetron-sputtered nc-TiC/a-C(AI) tough nanocomposite coatings [J]. Thin Solid Films, 2004, 467: 261–266.
- [30] MA T B, HU Y Z, WANG H. Molecular dynamics simulation of shear-induced graphitization of amorphous carbon films [J]. Carbon, 2009, 47: 1953–1957.
- [31] WENG K W, CHANG C L, WANG D Y. Effect of ion energy on degradation of diamond-like carbon films exposed to high-energy bombardment from an ion implanter [J]. Diamond Relat Mater, 2002, 11: 1447–1453.
- [32] TANAKA A, SUZUKI M, OHANA T. Friction and wear of various DLC films in water and air environment [J]. Tribol Lett, 2004, 17: 917–924.
- [33] SCHARF T W, SINGER I L. Role of the transfer film on the friction and wear of metal carbide reinforced amorphous carbon coatings during run-in [J]. Tribol Lett, 2009, 36: 43–53.

不同 Ti 靶电流对 Ti 掺杂类石墨碳膜的结构和性能的影响

王永欣^{1,2}, 王立平¹, 薛群基¹

1. 中国科学院 兰州化学物理研究所, 固体润滑国家重点实验室, 兰州 730000;

2. 中国科学院 研究生院, 北京 100039

摘要: 利用磁控溅射的方法成功制备 Ti 掺杂类石墨碳(Ti-GLC)膜。采用拉曼光谱、X 射线光电子谱(XPS)、扫描电子显微镜(SEM)、原子力显微镜(AFM)、纳米压痕仪和球盘式摩擦机分别表征不同 Ti 靶电流下制备的 Ti-GLC 膜的成分、结构和性能。随着 Ti 靶电流的增加, 薄膜中 sp² 键的比率和 Ti 含量增加, 同时薄膜的硬度和内应力也增大, 但较高的 Ti 靶电流将会促使薄膜产生鳞片状结构从而使其变疏松。较少的 Ti 掺入量可以降低 GLC 膜的干摩擦因数, 纯 GLC 膜在水润滑条件下的摩擦因数最低。在较低 Ti 靶电流下制备的 Ti-GLC 膜在干摩擦及水润滑条件下均具有较高的抗磨性能。

关键词: Ti 掺杂类石墨碳膜; 微观结构; 摩擦学性能; 靶电流

(Edited by LI Xiang-qun)